ISSN: 3092-8729 | e-ISSN: 3092-8737

ACJPAS

https://acjpas.acu.edu.ng

VOL. 5, NO. 2 2026

# Ajayi Crowther Journal of Pure and Applied Sciences

DOI: https://doi.org/10.56534/acjpas.v5i2

*A publication of the Faculty of Natural Sciences, Ajayi Crowther University*

ISSN: 3092-8729 | e-ISSN: 3092-8737

Ajayi Crowther Journal of Pure and Applied Sciences
https://acjpas.acu.edu.ng

Ajayi Crowther J. Pure Appl. Sci. 2026, 5(2), 57-67.
https://doi.org/10.56534/acjpas.v5i2.204


*Article*

# Ionospheric Response to the Strong Geomagnetic Storm of January 2025 at African Equatorial Stations

**Gbenga Akinpelumi Akinyemi[1]*, Saeed Abioye Bello[2], Abdullahi Kikelomo Kazeem[3], Modupe Eunice Sanyaolu[1], and Oladunjoye Peter Olabode[4]**

[1] Department of Physical Sciences, Redeemer's University, P.M.B. 230 Ede, Osun State, 232102 Nigeria; akinyemia@run.edu.ng (G.A.A.), sanyaolum@run.edu.ng (M.E.S.)

[2] Department of Physics, University of Ilorin, Nigeria; bello.sa@unilorin.edu.ng (S.A.B.)

[3] Department of Physics, Edo State University Iyamho, Edo State, Nigeria; k6abdul@yahoo.com (A.K.K.)

[4] Department of Geophysics, Federal University, Oye-Ekiti, Ekiti State, Nigeria; oladunjoye.olabode@fuoye.edu.ng (O.P.O.)

*Corresponding Author: G.A. Akinyemi (akinyemia@run.edu.ng)

***Article history:*** *Received: Apr. 8, 2026, Revised: May 10, 2026, Accepted: May 20, 2026, Published: Jun. 19, 2026.*

## Abstract

Total electron content (TEC) measurements from two International Global Navigation Satellite System (GNSS) Service (IGS) stations were utilised to investigate how the equatorial ionosphere responded to the strong geomagnetic storm of 1 January, 2025. The stations and their respective geographical coordinates are Libreville, Gabon (0.354° N, 9.672° E) and Mbarara, Uganda (0.601° S, 30.738° E), respectively representing the western and eastern parts of the African equatorial sector. In the storm's main phase, no significant ionospheric perturbation was observed at either station. However, during the recovery phase, Libreville exhibited exclusively a nighttime negative storm phase, while Mbarara exhibited both positive and negative phases, indicating marked longitudinal asymmetries in ionospheric response. These differences could be associated with the modulation of F-region dynamics by local electrodynamic processes, such as disturbance dynamo and prompt penetration electric fields, and storm-induced thermospheric composition changes.

**Keywords:** Geomagnetic storm, Ionospheric response, Ionospheric TEC, Equatorial ionosphere, Longitudinal asymmetry

## 1. Introduction

Prolonged periods of strong southward orientation of the Interplanetary Magnetic Field (IMF-Bz) will permit the transfer of energetic particles from the solar wind into the magnetosphere–ionosphere-thermosphere (M-I-T) coupled system (Gonzalez et al. 1999; Kumar et al. 2005). This injected particles, regardless of solar cycle phase (Ljiljana, 2016), perturb the ionosphere by altering the ionospheric plasma distribution (Chakraborty et al., 2015) and causing its variation to depart from the quiet-time regular diurnal patterns, primarily controlled by solar radiation. These global, large-scale temporal disturbances of the M-I-T system are generally called geomagnetic storms (Dungey, 1961; Retterer and Kelley, 2010; Schunk and Nagy, 2000). Among several disturbances within M-I-T system, such as substorms, sudden storm commencements, and the disturbance polar type 2 (DP2) current systems, geomagnetic storms have been observed to constitute the largest-scale and most prolonged global perturbations (Nagatsuma, 2002; Ljiljana, 2016). Some geomagnetic storms begin with "a sudden commencement (SC)" characterized by an abrupt increment in the geomagnetic field, resulting from

the magnetospheric compression by the dynamic pressure of the solar wind, while some commence gradually without initial sharp increment in the magnetic field. Geomagnetic storms undergo different phases (Kumar et al.,2005). The "main phase" is a period of progressive decrement in the Dst index values to the lowest. During this phase, because of the orientation of the Bz, which is predominantly southward, energy is efficiently transferred into the magnetosphere by the solar wind (Tsurutani et al.,2004). The period when Dst returns to its original values is called the "recovery phase". It is the period of minimum energy input, when geomagnetic activity weakens (Schunk and Nagy, 2000). Recovery phase is typically more gradual than the main phase and may last for several hours or even days (Trusutani, 2001).

Coronal mass ejection (CME) and coronal holes (Nagatsuma, 2002; Guo et al., 2011; Lepping et al., 2015; Gonzalez et al., 1994; Tsurutani et al., 2011; Abe et al., 2023) are the major sources of geomagnetic storms. Prompt penetration electric field (PPEF) (Nishida, 1968; Somayajulu, et al., 1987; Sastri et al., 1992) and the disturbance dynamo electric field (DDEF) (Blanc and Richmond, 1980; Chakraborty et al., 2015) are the principal origins of the perturbation of the ionospheric currents and electric fields, during geomagnetic storm. During an abrupt southward turn of IMF-Bz, almost instantly (time scale < 1h) (Kelley et al., 1979; Kikuchi et al., 1996; Tsurutani et al., 2008), electric field of the solar wind is mapped down to the equatorial ionosphere via PPEF to produce a strong dawn-to-dusk electric fields and a total increase of the magnetospheric convection.

These dawn-to-dusk electric fields significantly influence the electrodynamics of the equatorial ionosphere. PPEF is eastwardly oriented during the day and westwardly oriented at nighttime, hence strengthening the eastward dynamo electric field during the day. PPEF enhances the dayside equatorial ionosphere, particularly during the storm main phase, therefore, contributing to positive ionospheric response. (Maruyama et al., 2004; Tsurutani et al., 2004; Zhao et al., 2005). DDEF arises more gradually (time scale, from ~ 2 h to ~30 h) (Blanc and Richmond 1980; Fejer and Scherliess, 1997) from storm-time thermosspheric wind-driven dynamo processes. It is westward during the day, but turns eastward at night, thereby opposing and weakening the eastward dynamo electric field during daytime, therefore, more often, leading to TEC depletion in the dayside ionosphere (Tsurutani et al., 2004; Galav et al., 2011; Paul et al., 2018), particularly in the recovery phase. Nevertheless, Huang et al., (2005) reported that steady southward (or northward) IMF Bz (several hours) can produce enhanced dayside eastward (or westward) electric field at low latitudes. The phenomenon they referred to as "long-period enhancement of the electric field of the ionospheric". At the equator, neutral winds could raise the F-region plasma along magnetic field lines to higher heights where ion-electron recombination rate is slower, thereby altering the neutral composition, contributing to positive ionospheric storm effects (Fuller-Rowell et al., 1994). However, the same neutral winds transport molecular-rich air towards the equator, which can cause $O/N_2$ ratio to reduce and contributing to negative ionospheric storm effect. Additionally, the joule heating can transport the atmospheric gravity waves in the direction of the equator as travelling atmospheric disturbances (TADs). The interaction of the TADs with the ionosphere produces travelling ionospheric disturbances (TIDs) (Fagundes et al., 2016; de Abreu et al., 2010). TIDs typically produce wave-like perturbation in TEC.

One of the most common measurable and globally available ionospheric parameters is TEC (Buonsanto 1999; Danilov 2001; Akala et al., 2013). TEC serves as a proxy for the ionosphere because, by definition, it is the quantity of free electrons integrated along the path of a signal, from a satellite to a receiver on the ground (Davies and Hartman, 1997). Since ionospheric plasma density and distribution are significantly modified during geomagnetic storms (Fejer & Scherliess 1997), TEC is therefore an effective tool for monitoring and quantifying storm-time ionospheric responses. Global Positioning System (GPS) signals experience delay from ionospheric electrons as they travel to the ground receiver (Laboratories, 2017). This propagation delay is directly proportional to TEC (Olwendo et al., 2016; Noja et al., 2013), therefore, any variation in TEC raises great concerns (Galav et al., 2010).

Despite the significant electrodynamic variability of the African equatorial ionosphere and the consequent threats to navigation and communications systems (Akala et al., 2010), ionospheric study in this longitude sector has so far received comparatively less attention than other sectors such as North

America, Europe, and East Asia. This disparity is largely due to a dearth of data owing to the relatively sparse distribution of ionospheric observatories (Mendillo and Klobuchar, 2006). Consequently, to deepen our understanding of the dynamic nature of the ionosphere over the region and its implications for GNSS applications, continuous investigations of storm-time TEC response become necessary. Past studies on this subject abound in the literature. For instance, Joshua et al., (2018) studied the storm time response during the storm of April, 2010. They observed abrupt daytime enhancement in both TEC and peak electron density, which were attributed to the PPEFs. Namgaladze et al., (2000) investigated how the ionosphere responded to the geomagnetic storm of 25 January, 1974. They proposed large-scale neutral wind circulation and the TIDs passage as the cause of a positive ionospheric storm phase. de Abreu, et al., (2010) attributed the daytime positive ionospheric response of the recovery phase of the storm of April, 2000 to the meridional wind. Amabayo and Cilliers, (2013) studied response of the ionosphere over South Africa to the storms of March and April, 2001 and September, 2002. The observed positive and negative responses were largely attributed to TIDs which were identified as the driving mechanism that caused the perturbations. Paul et al., (2020) studied ionospheric response to the geomagnetic storm of 20 December, 2015. The observed large TEC enhancement in the course of the main phase of the storm for low-latitude and mid-latitude stations alike, was linked to the PPEF. In a study by Aol et al., (2023), the ionospheric response to the geomagnetic storm of 02–06 November 2021 was investigated using a combination of ground-based and satellite observations across selected low-latitude stations. The findings indicated a consistent positive ionospheric storm response across all the longitudinal sectors considered. The observed enhancements were interpreted as being influenced by prompt penetration electric fields storm-time neutral wind uplift processes, and disturbance dynamo electric fields.

The overall TEC enhancements over three equatorial stations during the main phase of the storm of 25 October as observed by Akinyemi et al., (2021) were attributed to enhancements in the electric field, which in turn produced prompt penetration effect.

This study aims to investigate the longitudinal variations in the ionospheric response to geomagnetic storm activity over the African sector. It presents a comparative analysis across equatorial stations, with particular emphasis on the differences in ionospheric response between the eastern and western regions.

## 2. Data and Methods

Two different datasets were utilized to carry out this study. The first comprises ionospheric total electron content (TEC) measurements obtained from two International GNSS Service stations. These stations are NKLG00GAB located in Libreville, Gabon (0.354° N, 9.672° E) and MBAR00UGA in Mbarara, Uganda (0.601° S, 30.738° E), representing the western and eastern extents of the African equatorial longitude sector examined.

The second dataset consists of solar wind and geomagnetic parameters obtained from the OMNIWeb Data Explorer. The parameters considered include the interplanetary magnetic field Bz component (IMF-Bz, nT), interplanetary electric field (IEFy, mV/m), solar wind speed (Vp, km/s), plasma temperature (K), plasma pressure (nPa), disturbance storm time index (Dst, nT), and planetary K index (Kp).

TEC variations are presented in universal time (UT) to aid comparison with geomagnetic indices. However, interpretation of ionospheric response is carried out in local solar time (LT), computed as LT = UT + (longitude/15). Accordingly, NKLG00GAB corresponds to UT + 0 h 39 min, while MBAR00UGA corresponds to UT + 2 h 03 min. Therefore, for instance, if UT is 02:00, it will be 02:39 LT and 04:03 LT in Libreville, Gabon and Mbarara, Uganda respectively.

Dual-frequency GPS observables in Receiver Independent Exchange (RINEX) format were obtained from the NASA Crustal Dynamics Data Information System (CDDIS) for the years 2024 and 2025.

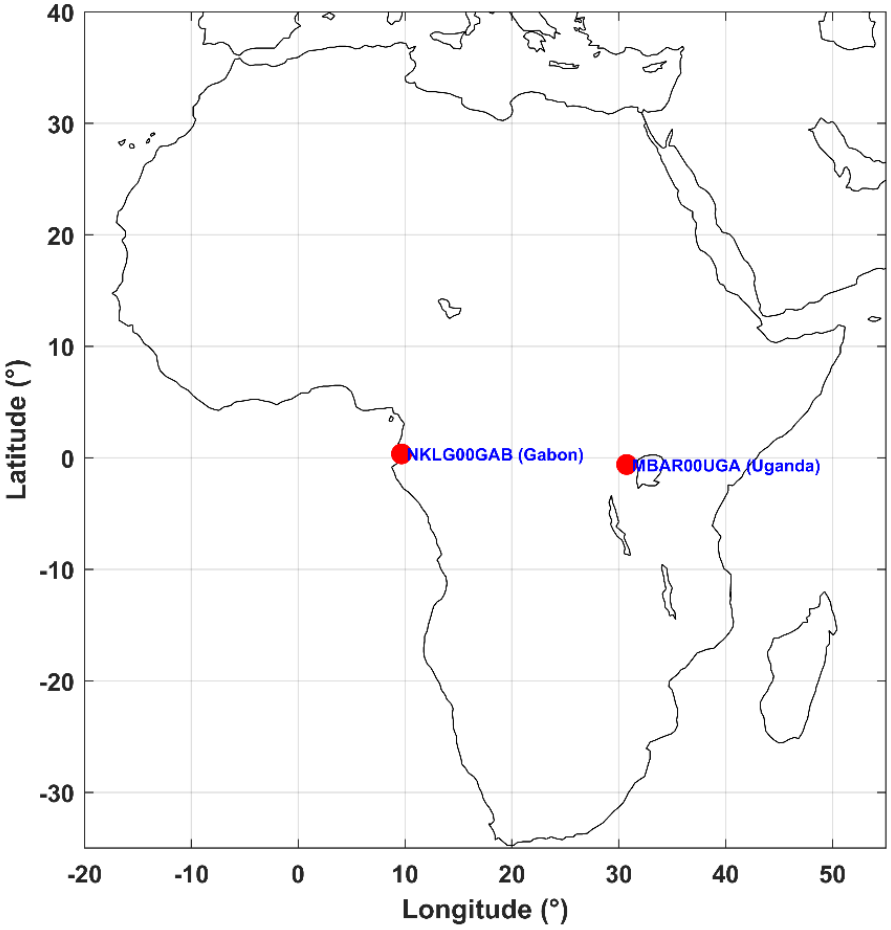


**Figure 1**. Map of Africa showing the locations of the GPS stations NKLG00GAB (Gabon; 0.354°N, 9.672°E) and MBAR00UGA (Uganda; 0.601°S, 30.738°E), which were used in the present analysis.

The estimation of TEC is based on the ionosphere the dispersive nature of the ionosphere, which causes radio signals to experience a frequency-dependent delay in group propagation and an advance in carrier phase (Adebiyi et al., 2014; Adebiyi et al., 2016).

By using this principle, TEC can be derived from dual-frequency GPS measurements, particularly the L1 (1575.42 MHz) and L2 (1227.60 MHz) carrier signals.

The resulting quantity, known as slant TEC ($TEC_s$), represents the integrated electron density along the signal path between the satellite and the ground receiver. It is determined through the combination of carrier phase and pseudorange (code) observations.

To eliminate the influence of satellite geometry and signal path length, $TEC_s$ is converted to vertical TEC ($TEC_v$). This conversion requires correction for instrumental biases as well as the application of a mapping function which accounts for the satellite elevation angle. The vertical TEC is expressed as:

$$TEC_v = \frac{TEC_S - (b_R + b_S)}{S(E)} \qquad 1$$

where $b_R$ and $b_S$ represent the receiver and satellite Differential Code Biases (DCB), respectively. S(E) is the obliquity factor (or slant factor), which is a function of the zenith angle (z) at the Ionospheric Pierce Point (IPP).

The obliquity factor is modeled as:

$$S(E) = \frac{1}{\cos z} = -\left(\frac{R_E \cos E}{R_E + h_s}\right)^{2^{-1/2}} \qquad 2$$

In this equation,$R_E$ is the Earth's radius, $E$ represents the satellite's elevation angle in degrees, while $h_s$ stands for the ionosphere's effective height.

The raw GPS RINEX files were processed using the GPS-TEC application software developed by Gopi Krishna Seemala at the Institute of Scientific Research, Boston College, USA (Gopi, 2023), following established protocols that included applying a 30° elevation mask to reduce multipath and troposcatter errors, assuming an effective ionospheric pierce point height ($h_s$) of 350 km, correcting satellite biases ($b_S$) with data from the Center for Orbit Determination in Europe (CODE), estimating receiver bias ($b_R$) through a 2σ iterated average of diurnal minimum values, and deriving quiet-time monthly averages from the five internationally quietest days identified by the GFZ German Research Centre for Geosciences.

In order to quantify the storm-time ionospheric response, the background TEC was estimated as mean of the five geomagnetically quietest days of January 2025. The percentage deviation of TEC was then computed following Abe et al., (2013, 2017)

$$\%\Delta TEC = \frac{TEC_{storm} - TEC_{quiet}}{TEC_{quiet}} \times 100 \qquad 3$$

and evaluated for the actual day of storm as well as two days before and two days after the storm. where:

$\%\Delta TEC$ = *Percentage deviation in TEC during storm conditions relative to quiet-time conditions.*
$TEC_{storm}$ = *Total Electron Content measured during the geomagnetic storm period.*
$TEC_{quiet}$ = *Background Total Electron Content measured during geomagnetically quiet conditions*.

From equation 3, positive values of % ΔTEC represent positive ionospheric storm while negative values represent negative ionospheric storm (Buonsanto, 1999). According to Cander, (2016), an ionospheric storm is said to be geomagnetic storm-driven if % ΔTEC of ±25% is exceeded for more than three hours consecutively. Whereas, moderate deviations in TEC (on the order of ±25%) may indicate the ionospheric natural day-to-day variability. The natural day-to-day variability of the ionosphere may arise from a combination of dynamical and external processes, including thermospheric neutral winds (both zonal and meridional), atmospheric tides, and gravity waves propagating from the lower atmosphere. These gravity waves are often generated by tropospheric convection and localized heating. (Kumar et al., 2005).

**3. Results**

Figure 2a-e presents the temporal variations in interplanetary parameters and geomagnetic indices associated with the storm of 1 January, 2025.

From the Figure 2, on 31 December 2024, the Dst index exhibited a sudden positive excursion from -3 nT at 16 UT to 14 nT and 17 nT at 16 and 17 UT, respectively, indicating a sudden storm commencement (SSC) (the green arrow in panel b). Thereafter, Dst began to decrease, reaching -30 nT at 01–02 UT on 1 January 2025, indicating the onset of the main phase. Following small fluctuations (−29 nT at 03 UT and −22 nT at 04 UT; see blue arrow in panel b), the Dst index decreased progressively, reaching a minimum of −212 nT at 16 UT on 1 January. This marks the end of a prolonged main phase lasting approximately 21 hours and characterizes the event as an intense geomagnetic storm.

This development is consistent with the pronounced southward turning of the IMF Bz commencing around 19 UT on 31 December, which later attained a minimum value of −21.5 nT. The timing also coincides with the peak of the interplanetary electric field along y-axis (IEFy), which reached about 10.36 mV/m at 16 UT on 1 January. Moreover, the Kp index reached a maximum value of 8 at minimum Dst, while the solar wind speed increased to a peak value of about 520 km/s at about 17 UT while the dynamic pressure fluctuated between positive values and reached a minimum near the Dst minimum.

This observation is typical of CME-driven storms where the ring current enhancement is primarily controlled by prolonged southward IMF Bz within the magnetic cloud, and not by dynamic pressure. The recovery phase commenced around 17 UT, roughly one hour after the main phase ended, and was marked by a gradual increase in Dst accompanied by a decline in the Kp index. The Figure shows that despite the fact that Dst reached a minimum, the solar wind speed did not show a corresponding decline, but rather remained elevated, indicating that the storm recovery phase was majorly controlled by ring current decay processes rather than by an immediate reduction in solar wind speed. It could also be noted from the Figure that the wind temperature rose sharply at SSC and fluctuated thereafter, reaching a relatively lower value at Dst minimum than at SSC or during the recovery phase. It was noted that the IMF Bz and IEFy exhibited frequent polarity reversals throughout the interval under investigation.

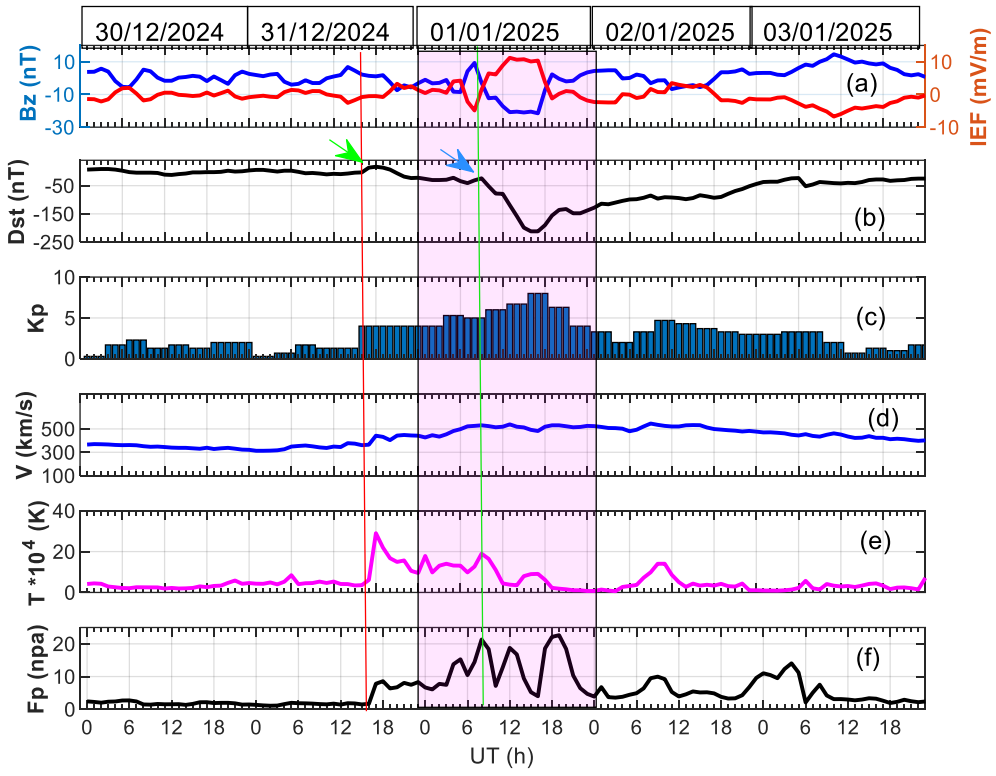


**Figure 2:** Time series of interplanetary parameters and geomagnetic indices during the intense storm of 1 January 2025. Panels show: (a) IMF Bz (nT) and IEFy (mV/m), (b) Dst (nT), (c) Kp index, (d) solar wind speed, V (km/s), (e) solar wind temperature (K), and (f) solar wind dynamic pressure, FP (nPa).

Figure 3 presents the diurnal TEC variations (red curves) from 30 December 2024 to 03 January 2025 (covering two days before, the storm day, and two days after), together with the average TEC of the five quietest days in January 2025 (black curves). Results are shown for (a) Libreville (NKLG) and (b) Mbarara (MBAR), while (c) and (d) show the corresponding hourly percentage deviations from quiet-time TEC at NKLG and MBAR, respectively.

From the Figure, during the main phase of the storm (20:00 UT on 31 December to 16:00 UT on 1 January), Δ%TEC at NKLG remained within ±25%, indicating the absence of an ionospheric disturbance associated with the activity of geomagnetic storm, according to the criterion of Cander

(2016). Whereas, at MBAR, brief excursions beyond the ±25% threshold were observed during the night period (+27% at 22 LT and −31% at 02–03 LT); however, these disturbances were not sustained for more than two consecutive hours and therefore do not meet the Cander (2016) definition of an ionospheric storm. During the recovery phase, at NKLG, Δ%TEC fell well below -25% for six consecutive hours, indicating a significant negative phase. The depletion in TEC became evident from 22:39 LT on 1 January to 03:39 LT on 2 January, with depletion ranging from ~-37% at 02:39 LT on 2 January to ~-70% at 23:39 LT on 1January. Thereafter, Δ%TEC varied within ±25% for the remaining period considered in this study. At MBAR, the TEC response during the recovery phase showed a multi-phase pattern marked by an intense four-hour positive phase between 19:00 LT and 22:00 LT on 1 January, with a maximum enhancement of ~67% at 21:00 LT, followed by a sudden transition into a seven-hour negative phase from 23:00 on 1 January to 04:00 LT on 2 January, with peak depletion of −70% at 01:00 LT. Thereafter, TEC recovered and entered a second positive phase which lasted almost to the end of 2 January, with maximum enhancement reaching ~70% at 06:00 LT. Interestingly, even on the second day of the minimum Dst, (3 January), a six-hour significant TEC depletion was still observed (from 01–06 LT), with the Δ%TEC values ranging between -29% and -44%, exceeding the ±25% storm threshold for more than three consecutive hours.

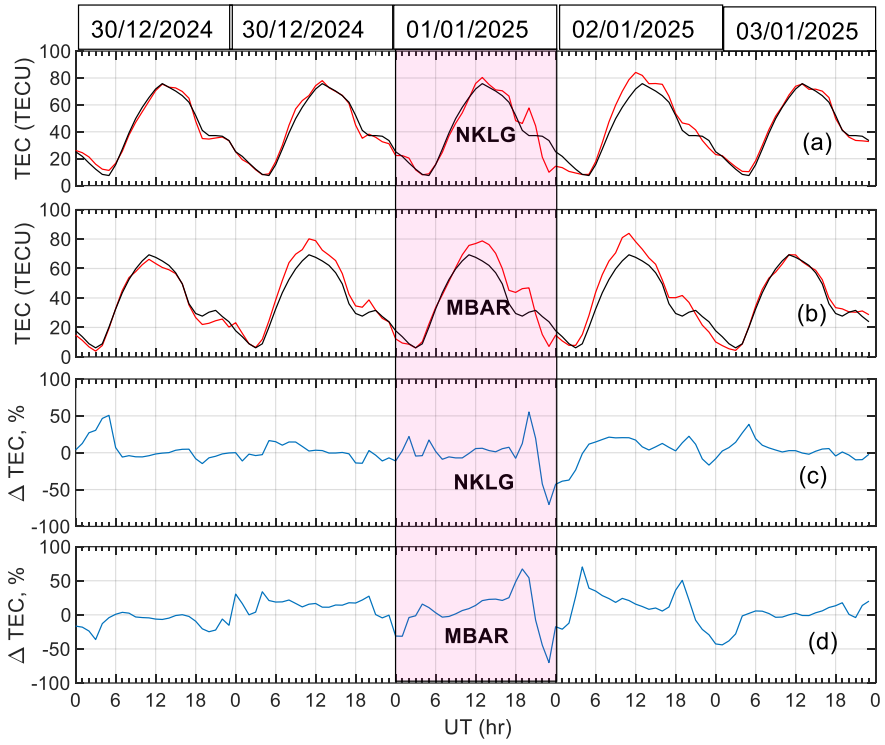


**Figure 3:** Variations of the mean TEC of the five quietest days of January 2025 (black curve) and TEC variations from 30 December, 2024 to 03, January, 2025 at (a) NKLG, (b) MBAR as well as ΔTEC at (c) NKLG and (d) MBAR.

## 4. Discussion

At equatorial latitudes, the background electric field is typically eastward during daytime and reverses to a weak westward direction at night. The daytime eastward field produces an upward E×B drift which lifts F-region plasma to higher altitudes, where reduced neutral density lowers recombination rates, leading to enhanced daytime electron density and TEC. On the other hand, the nighttime westward field produces a downward vertical plasma drift, which lowers the F-region plasma to regions where recombination rates are enhanced due to higher neutral particles, leading to a gradual decay of nighttime electron density and TEC. Since DDEF is typically westward during the day, it suppresses the quiet-time eastward ionospheric dynamo and reduces upward E×B plasma drift, forcing the plasma to remain at altitudes where recombination is strong, thereby contributing to daytime TEC depletion. During the night, DDEF reverses polarity and becomes eastward, opposing the weak quiet-

time westward field and promoting upward plasma drift leading to nighttime TEC enhancement. The observed negative phase between 22:39 LT and 03:39 LT at Libreville suggests that storm-time thermospheric composition changes and other factors must have played contributory roles. The prior daytime westward disturbance dynamo likely reduced the plasma reservoir before sunset, while reduced $O/N_2$ ratio enhanced nighttime recombination. Under such conditions, chemical loss exceeded transport effects, leading to sustained negative ionospheric storm phase. Storm-time auroral heating and global circulation drive thermospheric upwelling, which transports molecular-rich air to F-region altitudes, thereby reducing the $O/N_2$ ratio and enhancing ion–electron recombination, which reduces electron density and TEC at lower latitudes. Additionally, storm-time thermospheric winds can move plasma along geomagnetic field lines, pushing the F-region to lower altitudes where recombination rate is higher, reducing the electron density and TEC (Prölss, 1995; Danilov and Lastovicka, 2001; Danilov, 2013; Gordiyenko et al., 2025).

The ionosphere over Mbarara during the recovery phase of the geomagnetic storm exhibited a complex response, consisting of an initial short-lived positive phase between 19:00 and 22:00 LT on 1 January, followed by a pronounced negative phase between 23:00 LT and 04:00 LT, and finally a second positive phase that persisted almost into the morning of 2 January.

The marked enhancement (~67%) observed during the early recovery phase may be attributed to residual PPEFs driving upward E × B plasma drift at low latitudes; however, contributions from thermospheric composition changes and disturbance dynamo electric fields cannot be ruled out. Lei et al., (2018) explained that the observed prominent TEC enhancements which persisted during the storm recovery phase may be likely due to multiple mechanisms such as PPEF, neutral winds and thermospheric effects.

The sudden transition to a strong negative phase between 23:00 and 04:00 LT with a depletion of approximately −70%, suggests that thermospheric compositional disturbances and disturbance dynamo electric fields possibly became dominant following the initial electrodynamic forcing. Storm-time enhanced Joule heating at high latitudes generates strong pressure gradients that drives global thermospheric circulation and equatorward neutral winds (Fuller-Rowell et al., 1994). This can transport molecular-rich air toward low latitudes, reducing the thermospheric $O/N_2$ ratio, thereby increasing recombination rates in the F region and producing negative ionospheric storm effects (Fagundes et al., 2016; Prölss, 1995; Buonsanto, 1999). Also, storm-time neutral wind circulation can produce disturbance dynamo electric fields, which typically produce westward electric fields during the recovery phase. These fields usually reduce the upward E × B drift, thereby moving the F-region plasma to lower altitudes altitudes of higher recombination rates, further contributing to TEC depletion (Blanc and Richmond, 1980; Fejer and Scherliess, 1997).

The recovery of TEC followed by a second positive phase (~70% enhancement at 06:00 LT) suggests that the ionosphere gradually transitioned from an initial storm-time depletion phase dominated by disturbed thermospheric composition effects to a later phase influenced by plasma redistribution, vertical E × B drifts, and photochemical ionization processes. Storm-time winds can redistribute neutral composition globally. At equatorial and low-latitude regions, the convergence and downwelling of oxygen-rich air may increase the $O/N_2$ ratio and reduces ion recombination rates, thereby favoring enhanced electron density and TEC.

The observed recovery-phase prominence and the longitudinal contrast between Libreville and Mbarara indicate that ionospheric responses to geomagnetic storms in the African equatorial region are governed governed by the combined effects of disturbance dynamo electric fields and storm-induced thermospheric composition changes. The more persistent negative phase at Libreville suggests a more effective coupling between westward DDEF forcing and reduced $O/N_2$ ratio in the western sector, whereas the eastern sector reflects a more complex superposition of electrodynamic and compositional drivers.

## 5. Conclusion

The present work has investigated the response of the equatorial ionosphere to the strong geomagnetic storm of 1 January 2025. The following conclusions can be drawn from the results:

1. During the storm main phase, both stations exhibited relatively weak TEC disturbances despite the strong geomagnetic activity, implying that severe magnetospheric forcing does not always produce immediate strong ionospheric storm effects at equatorial latitudes.
2. Libreville experienced a prolonged negative ionospheric storm phase during the recovery period, with TEC depletion reaching ~−70%, suggesting strong thermospheric composition disturbances and enhanced recombination effects.
3. Mbarara exhibited a complex multi-phase ionospheric response consisting of alternating positive and negative storm phases, suggesting that several competing mechanisms operated simultaneously during the recovery phase.
4. The initial positive phase at Mbarara was likely associated with PPEFs and enhanced upward E×B plasma drifts, which temporarily increased TEC during the early recovery phase.
5. The subsequent strong negative phase at Mbarara suggests that thermospheric compositional disturbances and westward DDEFs later became dominant, reducing upward plasma transport and increasing recombination rates.
6. The persistence of TEC depletion into 3 January shows that ionospheric recovery can continue long after geomagnetic indices such as Dst begin to recover, indicating delayed thermosphere–ionosphere coupling effects.
7. The results confirm that recovery phase ionospheric disturbances can be more pronounced and complex than those occurring during the storm main phase, especially at equatorial and low-latitude regions. .

## References


Abe, O. E., Rabiu, A. B., & Adeniyi, J. O. (2013). Variability of foE in the equatorial ionosphere with solar activity. *Advances in Space Research, 51*(1), 69–75. https://doi.org/10.1016/j.asr.2012.08.010

Abe, O. E., Otero Villamide, X., Paparini, C., Ngaya, H. R., Radicella, S. M., & Nava, B. (2017). The storm-time assessment of GNSS-SBAS performance within low latitude African region using a testbed-like platform. *Astrophysics and Space Science, 362*, 1–8. https://doi.org/10.1007/s10509-017-3150-8

Abe, O. E., Fakomiti, M. O., Igboama, W. N., Akinola, O. O., Ogunmodimu, O., & Migoya-Orué, Y. O. (2023). Statistical analysis of the occurrence rate of geomagnetic storms during solar cycles 20–24. *Advances in Space Research, 71*(5), 2240–2251. https://doi.org/10.1016/j.asr.2022.10.033

Adebiyi, S. J., Odeyemi, O. O., Adimula, I. A., Oladipo, O. A., Ikubanni, S. O., Adebesin, B. O., & Joshua, B. W. (2014). GPS derived TEC and foF2 variability at an equatorial station and the performance of IRI-model. *Advances in Space Research, 54*(4), 565–575. https://doi.org/10.1016/j.asr.2014.03.026

Adebiyi, S. J., Adimula, I. A., Oladipo, O. A., & Joshua, B. W. (2016). Assessment of IRI and IRI-Plas models over the African equatorial and low-latitude region. *Journal of Geophysical Research: Space Physics, 121*, 7287–7300. https://doi.org/10.1002/2016JA022697

Akala, A. O., Oyeyemi, A. E., Somoye, E. O., Adeloye, A. B., & Adewale, A. O. (2010). Variability of foF2 in the African equatorial ionosphere. *Advances in Space Research, 45*, 1311.

Amabayo, E. B., & Cilliers, P. J. (2013). Multi-station observation of ionospheric irregularities over South Africa during strong geomagnetic storms. *Advances in Space Research, 51*, 754–771.

Akinyemi, G. A., Kolawole, L. B., Dairo, O. F., Willoughby, A. A., Abdulrahim, R. B., & Rabiu, A. B. (2021). The response of the equatorial ionosphere over Nigeria to a geomagnetic storm event. *Geomagnetism and Aeronomy, 61*(4), 647–657.

Aol, S., Habyarimana, V., Mungufeni, P., et al. (2023). Ground and space-based response of the ionosphere during the geomagnetic storm of 02–06 November 2021 over the low-latitudes across different longitudes. *Advances in Space Research*. https://doi.org/10.1016/j.asr.2023.12.032

Blanc, M., & Richmond, A. D. (1980). The ionospheric disturbance dynamo. *Journal of Geophysical Research, 85*, 1669–1686.

Buonsanto, M. J. (1999). Ionospheric storms: A review. *Space Science Reviews, 88*, 563–601.

Chakraborty, M., Kumar, S., Birnin, K., & Ghosh, A. (2015). Effects of geomagnetic storm on low latitude ionospheric total electron content: A case study from Indian sector. *Journal of Earth System Science, 124*, 1115–1120.

Danilov, A. D. (2001). F-region reaction to magnetospheric storm. *Journal of Atmospheric and Solar-Terrestrial Physics, 63*, 441–449.

Davies, K., & Hartmann, G. K. (1997). Studying the ionosphere with global positioning system. *Radio Science, 32*, 1695–1703.

Danilov, A. D., & Lastovicka, J. (2001). Effects of geomagnetic storms on the ionosphere and atmosphere. *International Journal of Geomagnetism and Aeronomy, 2*, 209–219.

Danilov, A. D. (2013). Ionospheric F-region response to geomagnetic disturbances. *Advances in Space Research, 52*, 343–366.

de Abreu, A. J., Sahai, Y., Fagundes, P. R., Becker-Guedes, F., de Jesus, R., Guarnieri, F. L., & Pillat, V. G. (2010). Response of the ionospheric F-region in the Brazilian sector during the super geomagnetic storm in April 2000 observed by GPS. *Advances in Space Research, 45*, 1322–1329. https://doi.org/10.1016/j.asr.2010.02.003

Dungey, J. W. (1961). Interplanetary magnetic field and the auroral zones. *Physical Review Letters, 6*, 47–48.

European Space Agency Swarm Satellite Earth Observation Laboratories. (2017). *Swarm L2 TEC product description (Version 4.0).* https://earth.esa.int/eogateway/documents/20142/37627/

Fagundes, P. R., Cardoso, F. A., Fejer, B. G., Venkatesh, K., Ribeiro, B. A. G., & Pillat, V. G. (2016). Positive and negative GPS TEC ionospheric storm effects during the extreme space weather event of March 2015 over the Brazilian sector. *Journal of Geophysical Research: Space Physics, 121*(6), 5613–5625. https://doi.org/10.1002/2015JA022214

Fejer, B. G., & Scherliess, L. (1997). Empirical models of storm time equatorial electric field. *Journal of Geophysical Research: Space Physics, 102*, 24047–24056. https://doi.org/10.1029/97JA02164

Fuller-Rowell, T. J., Codrescu, M. V., Moffett, R. J., & Quegan, S. (1994). Response of the thermosphere and ionosphere to geomagnetic storms. *Journal of Geophysical Research: Space Physics, 99*(A3), 3893–3914.

Galav, P., Dashora, N., Sharma, S., & Pandey, R. (2010). Characterization of low latitude GPS-TEC during very low solar activity phase. *Journal of Atmospheric and Solar-Terrestrial Physics, 72*, 1309–1317. https://doi.org/10.1016/j.jastp.2010.09.017

Galav, P., Sharma, S., & Pandey, R. (2011). Study of simultaneous penetration of electric fields and variation of total electron content in the day and night sectors during the geomagnetic storm of 23 May 2002. *Journal of Geophysical Research: Space Physics, 116*, A12324.

Gonzalez, W. D., Tsurutani, B. T., & Clúa de Gonzalez, A. L. (1999). Interplanetary origin of geomagnetic storms. *Space Science Reviews, 88*, 529–562. https://doi.org/10.1023/A:1005160129098

Gonzalez, W. D., Joselyn, J. A., Kamide, Y., Kroehl, H. W., Rostoker, G., Tsurutani, B. T., & Vasyliunas, V. M. (1994). What is a geomagnetic storm? *Journal of Geophysical Research: Space Physics, 99*(6), 5771–5792.

Gordiyenko, G., Arikan, F., Litvinov, Y., & Zhiganbaev, M. (2025). Ionospheric response to the extreme geomagnetic storm of 10–11 May 2024 based on total electron content observations in the Central Asian and East Asian regions. *Atmosphere, 16*, 854.

Guo, J., Feng, X., Emery, B. A., Zhang, J., Xiang, C., Shen, F., & Song, W. (2011). Energy transfer during intense geomagnetic storms driven by interplanetary coronal mass ejections and their sheath regions. *Journal of Geophysical Research: Space Physics, 116*, A05106. https://doi.org/10.1029/2011JA016490

Huang, C.-S., Foster, J. C., & Kelley, M. C. (2005). Long-duration penetration of the interplanetary electric field to the low-latitude ionosphere during the main phase of magnetic storms. *Journal of Geophysical Research: Space Physics, 110*, A11309. https://doi.org/10.1029/2005JA011202

Joshua, B. W., Adeniyi, J. O., Oladepo, O. A., Doherty, P. H., Adimula, I. A., Olawepo, A. O., & Adebiyi, S. J. (2018). Simultaneous response of NmF2 and GPS-TEC to storm events at Ilorin. *Advances in Space Research*. https://doi.org/10.1016/j.asr.2018.03.031

Kelley, M., Fejer, B., & Gonzales, C. (1979). An explanation for anomalous equatorial ionospheric electric field associated with a northward turning of the interplanetary magnetic field. *Geophysical Research Letters, 6*(4), 301–304.

Kikuchi, T., Lühr, H., Kitamura, T., Saka, O., & Schlegel, K. (1996). Direct penetration of the polar electric field to the equator during a DP2 event as detected by the auroral and equatorial magnetometer chains and the EISCAT radar. *Journal of Geophysical Research: Space Physics, 101*, 17161–17173.

Kumar, S., Chandra, H., & Sharma, S. (2005). Geomagnetic storms and their ionospheric effects observed at the equatorial anomaly crest in the India region. *Journal of Atmospheric and Solar-Terrestrial Physics, 67*, 581–594.

Lei, J., Huang, F., Chen, X., Zhong, J., Ren, D., Wang, W., Yue, X., & Luan, X. (2018). Was magnetic storm the only driver of the positive ionospheric storm during 17–18 March 2015? *Journal of Geophysical Research: Space Physics, 123*(4), 3217–3232. https://doi.org/10.1002/2017JA024661

Lepping, R. P., Wu, C., & Berdichevsky, D. B. (2015). Yearly comparison of magnetic cloud parameters, sunspot number, and interplanetary quantities for the first 18 years of the Wind mission. *Solar Physics, 290*, 553–578. https://doi.org/10.1007/s11207-014-0622-7

Cander, L. R. (2016). Re-visit of ionospheric storm morphology with TEC data in the current solar cycle. *Journal of Atmospheric and Solar-Terrestrial Physics, 138–139*, 187–205. https://doi.org/10.1016/j.jastp.2016.01.008

Maruyama, T., Ma, G., & Nakamura, M. (2004). Signature of TEC storm on 6 November 2001 derived from dense GPS receiver network and ionospheric chain over Japan. *Journal of Geophysical Research: Space Physics, 109*, A10302.

Mendillo, M., & Klobuchar, J. A. (2006). Total electron content: Synthesis of past storm studies and needed future work. *Radio Science, 41*, RS5S02. https://doi.org/10.1029/2005RS003394

Nagatsuma, T. (2002). Geomagnetic storms. *Journal of the Communications Research Laboratory, 47*(3).

Namgaladze, A. A., Forster, M., & Yurik, R. Y. (2000). Analysis of the positive ionospheric response to a moderate geomagnetic storm using a global numerical model. *Annales Geophysicae, 18*, 461–477.

Nishida, A. (1968). Coherence of geomagnetic DP2 magnetic fluctuations with interplanetary magnetic variations. *Journal of Geophysical Research, 73*(17), 5549–5559.

Noja, M., Stolle, C., Park, J., et al. (2013). Long-term analysis of ionospheric polar patches based on CHAMP TEC data. *Radio Science, 48*(3), 289–301. https://doi.org/10.1002/rds.20033

Olwendo, O., Yamazaki, Y., Cilliers, P., Baki, P., & Doherty, P. (2016). A study on the variability of ionospheric total electron content over the East African low-latitude region and storm time ionospheric variations. *Radio Science, 51*, 1503–1518. https://doi.org/10.1002/2015RS005785

Paul, B., De, B. K., & Guha, A. (2018). Latitudinal variation of F-region ionospheric response during three strongest geomagnetic storms of 2015. *Acta Geodaetica et Geophysica, 53*, 579–606.

Paul, B., Gordiyenko, G., & Galav, P. (2020). Study of the low and mid-latitude ionospheric response to the geomagnetic storm of 20th December 2015. *Astrophysics and Space Science, 365*, 174. https://doi.org/10.1007/s10509-020-03884-5

Prölss, G. W. (1995). Ionospheric F-region storms. In H. Volland (Ed.), *Handbook of atmospheric electrodynamics* (Vol. 2, pp. 195–248). CRC Press.

Retterer, J., & Kelley, M. (2010). Solar wind drivers for low-latitude ionosphere during geomagnetic storms. *Journal of Atmospheric and Solar-Terrestrial Physics, 72*, 344–349.

Sastri, J. H., Ramesh, K. B., & Ranganath Rao, H. N. (1992). Transient composite electric field disturbances near the dip equator associated with auroral substorms. *Geophysical Research Letters, 19*, 1451–1454.

Schunk, R. W., & Nagy, A. F. (2000). *Ionospheres: Physics, plasma physics, and chemistry*. Cambridge University Press.

Somayajulu, V. V., Reddy, C. A., & Viswanathan, K. S. (1987). Penetration of magnetospheric convective electric field to the equatorial ionosphere during the substorm of March 22, 1979. *Geophysical Research Letters, 14*(8), 876–879.

Tsurutani, B. T. (2001). The interplanetary causes of magnetic storms, substorms and geomagnetic quiet. In I. A. Daglis (Ed.), *Space storms and space weather hazards* (pp. 103–130). Kluwer Academic Publishers.

Tsurutani, B. T., Echer, E., Guarnieri, F. L., & Gonzalez, W. D. (2011). The properties of two solar wind high speed streams and related geomagnetic activity during the declining phase of solar cycle 23. *Journal of Atmospheric and Solar-Terrestrial Physics, 73*, 164–177. https://doi.org/10.1016/j.jastp.2010.04.003

Tsurutani, B. T., Mannucci, A. J., Iijima, B., Abdu, M. A., Sobral, J. H. A., Gonzalez, W. D., Guarnieri, F. L., Tsuda, T., Saito, A., Yumoto, K., Fejer, B. G., Fuller-Rowell, T. J., Kozyra, J. U., Foster, J. C., Coster, A. J., & Vasyliunas, V. M. (2004). Global dayside ionospheric uplift and enhancement associated with interplanetary electric fields. *Journal of Geophysical Research: Space Physics, 109*, A08302. https://doi.org/10.1029/2003JA010342

Tsurutani, B. T., Verkhoglyadova, O. P., Mannucci, A. J., et al. (2008). Prompt penetration electric fields (PPEFs) and their ionospheric effects during the great magnetic storm of 30–31 October 2003. *Journal of Geophysical Research: Space Physics, 113*(A5), A05311. https://doi.org/10.1029/2007JA012879

Zhao, B., Wan, W., & Liu, L. (2005). Responses of equatorial anomaly to the October–November 2003 superstorms. *Annales Geophysicae, 23*, 693–706.

**Funding**
Not applicable.

**Institutional Review Board Statement**
Not applicable.

**Informed Consent Statement**
Not applicable.

**Acknowledgements**
Not applicable.

**Conflict of Interest**
The author declared no conflict of interest in the manuscript.

**Authors' Declaration**
The author(s) hereby declare that the work presented in this article is original and that any liability for claims relating to the content of this article will be borne by them.

**Author Contributions**
Conceptualization – G.A.A.; Design – G.A.A.; Supervision – S.A.B. Resources – G.A.A., S.A.B., M.E.S, A.K.K. Materials – S.A.B., A.K.K. Data Collection and/or Processing – S.A.B. Analysis and/or Interpretation – G.A.A. Literature Search – G.A.A., S.A.B., M.E.S. Writing – G.A.A. Critical Reviews – G.A.A., S.A.B. A.K.K., M.E.S., O.P.O.

*Cite article as:*

Akinyemi, G.A., Bello, S.A., Kazeem, A.K., Sanyaolu, M.E. & Olabode, O.P. (2026). Ionospheric Response to the Strong Geomagnetic Storm of January 2025 at African Equatorial Stations. *Ajayi Crowther Journal of Pure and Applied Sciences, 5*(2), 57–67. https://doi.org/10.56534/acjpas.v5i2.204